Journal of Power Sources 196 (2011) 7470–7480

Contents lists available at ScienceDirect

Journal of Power Sources

journal homepage: www.elsevier.com/locate/jpowsour

Low Pt-loading Ni–Pt and Pt deposits on Ni: Preparation, activity and investigation of electronic properties

Sonja A. Francis, Steven H. Bergens*

Department of Chemistry, University of Alberta, Edmonton, Alberta T6G 2G2, Canada

ARTICLE INFO

Article history:
Received 29 March 2011
Received in revised form 29 April 2011
Accepted 6 May 2011
Available online 18 May 2011

Keywords:
Platinum
Nickel
Co-deposition
2-Propanol
Alkaline
Direct alcohol fuel cell

ABSTRACT

A unique, self-limiting, galvanostatic deposition was used to synthesize co-deposits of Ni and Pt onto nickel substrates from sonicated solutions of 0.2 M $NiCl_2$ in 2.0 M NH_4Cl, with a platinum blacked counter electrode as the sole platinum source. Depositions of only Pt onto the nickel substrates were also performed using this method. Cyclic voltammetry, chronoamperometry, carbon monoxide stripping voltammetry, inductively coupled plasma mass spectrometry, scanning electron microscopy, energy-dispersive X-ray spectroscopy and X-ray photoelectron spectroscopy were performed on the deposits. Results demonstrate that, due to the self-regulating nature of this deposition, the Pt-content of the co-deposits does not exceed 8 mol% loading and most of the Pt resides at or near the catalyst surface. The surface atom normalized activities of the co-deposits (Ni–Pt on Ni foam) and Pt-only deposits (Pt on Ni foam) were up to 37 times higher than platinum black towards 2-propanol electro-oxidation in base at 500 mV vs. RHE; the order of activity is Pt on Ni foam ≫ Ni–Pt on Ni foam > Pt black. The Ni–Pt and Pt on Ni foam catalysts are more active than Pt black at >500 mV mainly via the bi-functional mechanism and some electronic effects. The Pt on Ni foam was the most superior catalyst due to a combination of geometric and bi-functional effects.

1. Introduction

Direct alcohol fuel cells (DAFCs) are promising power sources for portable devices due to their simple fuelling systems [1], relatively low operating temperatures [2], and higher energy densities than hydrogen [3]. DAFCs are also used as alcohol sensors [4,5]. Various alcohols including methanol (MeOH) [6], ethanol [7], ethylene glycol [8], glycerol [9], and *n*-propanol [10] have been evaluated as potential fuels for DAFCs. MeOH is the most studied due to its availability, lack of C–C bonds, and good electrochemical activity. The interest in 2-propanol (2-PrOH) has recently increased [1,11–19] because 2-PrOH is less prone to anode poisoning than MeOH at moderate current densities, it has lower electro-oxidation onset potentials over Pt and Pt–Ru [1,11], it is less toxic [20], and it has a higher boiling point. For example, a Nafion®-based DAFC with a Pt–Ru anode catalyst operated on 2-PrOH with ~200 mV higher cell voltage at 120 mA cm^{-2} than MeOH [12]. The 2-PrOH cell, however, lost activity from anode poisoning at higher currents. Similarly, a liquid electrolyte alkaline fuel cell operated on 2-PrOH with higher open-circuit voltage, and with markedly higher power outputs and stability at cell voltages over 0.5 V than MeOH [1].

The electro-oxidation of 2-PrOH in alkaline electrolytes has been reported over Pd [12,13], Pd–Au [14], Au [15], Ru [16], Pt–Rh [13], Pt–Ru [17] and Pt [17–19]. The mechanism of 2-PrOH oxidation over Pt in base is proposed to change with potential as follows:

$$CH_3CHOHCH_3 + 2OH^- \rightarrow CH_3COCH_3 + 2H_2O + 2e^- \quad (1)$$

$$CH_3COCH_3 + 16OH^- \rightarrow 3CO_2 + 11H_2O + 16e^- \quad (2)$$

The electro-oxidation to acetone (Eq. (1)) commences at lower potentials (~−750 mV to −600 mV vs. SHE, pH 14), and with higher currents than the electro-oxidation of MeOH. This 2-electron oxidation does not involve intermediates that strongly poison the catalyst surface. As the potential is increased, however, acetone and other intermediates do strongly adsorb to Pt, impeding the oxidation of 2-PrOH until they are oxidised at high potentials (Eq. (2)) [17].

Our group has shown that both ruthenium [17] and nickel [21] promote 2-PrOH electro-oxidation over Pt. Ru promotes the electro-oxidation over a wide range of potentials, while Ni primarily promotes at higher potentials. These enhancements in activity are likely due, in part, to the well-known bifunctional mechanism [2,22–25]. Indeed, small amounts CO were detected during the electro-oxidation of 2-PrOH [26], although the nature of the strongly adsorbed intermediates in acetone electro-oxidation are still under investigation. Some authors also suggest that oxidised nickel surfaces catalyze alcohol electro-oxidations [27].

* Corresponding author. Tel.: +1 780 492 9703; fax: +1 780 492 8231.
E-mail address: steve.bergens@ualberta.ca (S.H. Bergens).

0378-7753/$ – see front matter © 2011 Elsevier B.V. All rights reserved.
doi:10.1016/j.jpowsour.2011.05.011

To our knowledge, we are the only group that has reported the electro-oxidation of 2-PrOH over Ni–Pt [21]. Ni–Pt systems have been mostly studied as catalysts for the MEOH oxidation reaction (MOR) [27–33], and for the oxygen reduction reaction (ORR) [33–42]. The synthetic method, pre-treatment, structure and composition of theses catalysts all heavily influence their activity. For example, Ni–Pt catalysts with Pt-rich surfaces and Ni-rich subsurfaces are very active towards the ORR. Typical syntheses of these structures include atomic layer deposition [34], sequential chemical reduction of metal salts [35], and transmetalation [36]. Pre-treatments such as annealing [37] or potential cycling in acid [36,38] also form Pt-rich surfaces by surface segregation or by Ni dissolution. Theoretical [39] and experimental [40] results suggest that Ni shifts the Pt *d* band center away from the Fermi level and/or shifts the binding energy of Pt core electrons to lower values [43]. Early reports also suggested that the high activity of Pt_3Ni alloys towards the ORR resulted from weaker adsorption of OH and related species on Pt sites bordered by oxide-covered Ni [44–46]. Marković and Ross later demonstrated that sub-surface nickel weakened OH adsorption on Pt by an electronic effect [38,47]. They also provided strong evidence that adsorbed OH blocks the sites required for O_2 adsorption. Tegou et al. found that Pt–Ni structures prepared by transmetallation operated with high coverages by oxygen-containing species *and* with high ORR activity [36]. They suggested that the ORR is not controlled by the surface oxide coverage but by the dissociative adsorption of O_2, which is more facile on Pt–Ni due to electronic effects. Mu et al. reported that Ni–Pt catalysts with Ni oxide nano-islands on Pt (1 1 1) with subsurface Ni were very active towards both O_2 activation and CO oxidation [48]. These authors asserted that the Ni oxide islands are the sites for O_2 dissociation, and that the subsurface Ni enhanced CO oxidation over Pt. Antolini and co-workers found that the ORR activity of their carbon-supported Ni–Pt catalysts, synthesised by borohydride reduction of Ni and Pt salts, depended on the amount of alloyed Ni and not the composition of Ni [33].

The relationship between structure and MOR activity over Ni–Pt is less studied. Yang et al. asserted that the chemisorption of MeOH is facile when at least three neighbouring Pt atoms are in the correct crystallographic arrangement on the surface [28]. Such arrangements are more likely in Pt-rich surfaces. The bifunctional mechanism, however, is more likely to operate on alloy-type, bimetallic surfaces with more Ni–Pt contacts (synthesised, e.g. by chemical co-reduction of metal salts [27,29,30,33] or by co- and step-impregnation [31]). Papadimitirou et al. synthesised Ni–Pt coatings on Ni cores by galvanic displacement of Ni by Pt [32] followed by potential cycling between the limits of H_2 and O_2 evolution in acid, resulting in surfaces that were enriched in Pt. They concluded that surfaces with less than 50% Ni have low activity towards the MOR. This trend was also observed by Yang et al. on Ni–Pt catalysts made without deliberate surface enrichment in Pt by segregation or by potential sweeping in acid [28]. In contrast, Mathiyarasu et al. found that maximum activity towards the MOR occurred with 8% Ni in smooth films of Ni–Pt [49]. They proposed that higher percentages of Ni at the surface decreases the number of Pt sites required for MeOH adsorption. The influence of the structural differences between these catalysts on their activities requires further investigation [50,51]. Finally, Antolini et al. found that the activity of their carbon-supported Ni–Pt catalysts increased with increasing amounts of unalloyed NiO species [33], and suggested that the oxidised nickel aids the MOR by supplying Pt-CO with oxygen species.

The literature demonstrates that the structure and composition of Pt–Ni catalysts strongly influence their activities. We previously reported a novel galvanostatic, self-limiting co-deposition of Ni and Pt onto nickel gauze [21] using a Pt black counter electrode (CE) and a Ni gauze working electrode (WE) in aqueous solutions of $NiCl_2$ and NH_4Cl. Briefly, the deposition of Ni onto the WE, and the formation of Pt ions in solution from partial dissolution of the CE, are the dominant processes during the initial stages of the deposition. Subsequently, Pt and Ni are both deposited onto the WE until H_2 evolution over Pt becomes the dominant process, resulting in a sudden rise in E_{WE} above the Ni(0)/Ni(II) redox potential [21]. The Pt black CE is also passivated by the formation of surface oxides, preventing further dissolution of Pt into solution. The deposition is thereby self-limiting with respect to both metals, and it produces milligram-scale deposits with as low as 1.8 mol% of Pt. The majority of the Pt is on, or near the bimetallic surface of the deposit. As detailed in the previous paragraphs, such a structure is desirable as it not only allows for efficient utilization of the Pt, but it also it allows for bi-functional and/or electronic effects that can enhance the catalytic activity of these surfaces.

In this report, we extend the self-limited deposition to nickel foam as a substrate under ultra-sonification. We also achieved self-limiting depositions of only Pt, via exclusion of the nickel salt from the deposition solution. Ni foam was chosen due to its inherent high surface area and porosity and because it could function as catalyst substrate, current collector, and mechanical support [52–54]. We used ultra-sonification to increase mass transport to the electrode surface [55] and to create more durable deposits with relatively high surface areas [56]. We also present a more thorough characterisation of the deposits via scanning electron microscopy/energy dispersive X-ray spectroscopy (SEM/EDX) and X-ray photoelectron spectroscopy (XPS). The results of these characterizations are employed to interpret the relative activities of our catalysts towards 2-PrOH electro-oxidation in base.

2. Experimental

2.1. Preparation of electrodes

The support for the depositions consisted of either a 1 cm × 1 cm nickel foam (Goodfellow Cambridge Limited, 95% porosity, 95% purity) or nickel gauze (Alfa Aesar, 100 mesh woven from 0.1 mm wire, and 99.9% metal basis) with a 3 mm × 3 mm tab. The tab allowed insertion into a graphite rod handle protected from the electrolyte with Teflon tape. Prior to the deposition, the substrates were cleaned in 1% hydrogen peroxide (Fischer Scientific) followed by triply distilled water. The electro-deposition and all other electrochemical experiments were performed using an EG&G Princeton Applied Research Potentiostat/Galvanostat Model 273 controlled with EG&G PARC M270 software. The deposition apparatus consisted of a 10 cm × 2.5 cm diameter glass cylinder immersed in a sonicator bath (Core-Palmer Model 8890). The Ni–Pt depositions were carried out as described elsewhere [21], but with sonication instead of stirring. Briefly, a constant current of −0.1 A was applied between the substrate and the counter electrode in a 3-electrode cell with 30 mL of 0.2 M $NiCl_2$ Baker & Adamson) in 2.0 M NH_4Cl (Caledon). The 3-electrode cell comprised an Aldrich saturated calomel or $Ag/AgCl_2$ double junction reference electrode, a platinum blackened gauze as the counter electrode, and the pre-treated substrate as the working electrode. The counter electrode was a 2 cm × 2 cm Pt gauze (Alfa Aesar, 52 mesh woven from 0.1 mm wire, 99.9% metals basis) blackened in 1 wt% K_2PtCl_6 (Aithaca Chemical Corp.) in 1 M $HClO_4$ (Anachemia) or 2 wt% $H_2PtCl_6{\cdot}6H_2O$ (Alfa Aesar) in 1 M HCl (EMD Chemicals). No difference in results was observed with the different blackening methods. The real surface area of the gauze, calculated from the hydrogen under potential deposition peak in 1 M H_2SO_4, was more than 25,000 cm^2 assuming the charge associated with adsorbing a monolayer of hydrides is 210 $\mu C\,cm^{-2}$ with 77% efficiency. The potential of the counter electrode during the deposition was monitored by a Radio Shack

multimeter using Scope View version 1.08 software. The Pt depositions on nickel foam were performed in the same manner with the exclusion of $NiCl_2$ from the electrolyte.

The Pt blacked gauze used for activity comparisons was a 1 cm × 1 cm Pt gauze with a 3 mm × 3 mm tab for insertion into a graphite handle wrapped in Teflon tape to shield from the electrolyte. The gauze was blackened in 1 wt% K_2PtCl_6 in 1 M $HClO_4$ for 2 h, that is, the time for the solution to lose its yellow colour.

2.2. Characterization and activity of electrodes

SEM was performed on a Zeiss EVO MA 15 scanning electron microscope equipped with a Bruker Silicon Drift Detector for EDX. A Kratos Analytical Axis Ultra X-ray Imaging Photoelectron Spectrometer was used to run XPS. Both techniques were executed on freshly prepared samples rinsed with triply distilled water, then copiously with ethanol, and dried in a dessicator under vacuum overnight. XPS data fitting was performed using CASA XPS Software File version 1.0.0.1, and the binding energies of the peaks were calculated from the background-subtracted spectrum using an applied Shirley background. The spectra were calibrated to adventitious carbon at 284.8 eV. The intensity ratios of the Pt $4f_{7/2}$ and $4f_{5/2}$ peaks were set to the theoretical value of 4:3 and spin-orbit coupling was 3.3 eV; The Ni $3p_{3/2}$ and $3p_{1/2}$ peaks were set to have intensity ratios of 2:1 and separation of 1.9 eV [57]. The Pt peaks were assigned 10% asymmetry to account for the experimental line shape, while all other peaks were fitted with 30% Gaussian–Lorentzian curves.

Cyclic voltammetry and chronoamperometry were carried out under nitrogen (Praxair pre-purified) in 90 mL of 0.5 M NaOH (Alfa Aesar 99.99% semi-conductor grade) that was deaerated with nitrogen bubbling in the electrolyte for 10 min. The system comprised a 3-neck flask sealed with toluene-extracted septa punched with holes to support the electrode handles. The platinum blacked counter was isolated behind a glass tube with a 10 μm glass frit. A static reversible hydrogen electrode (RHE) in the supporting electrolyte was used as a reference point. All potentials are versus this reference unless stated otherwise. The working electrode was conditioned for 5 min at −400 mV prior to each experiment. The stabilised voltammogram (3rd cycle) of the working electrode was obtained between −100 and 425 mV at 10 mV s^{-1} at room temperature (22 °C). For the alcohol oxidation experiments, 6.9 mL of freshly distilled 2-PrOH (Fischer Scientific, ACS plus grade) was added to the 90 mL of the electrolyte at 60 °C and the mixture purged a further 5 min with N_2. A dry ice/acetone condenser was used to minimize evaporation loss of the alcohol. Cyclic voltammograms in the presence of 2-PrOH were collected as above but at 60 °C. Chronoamperometric responses were collected by stepping to the desired potential for 15 min. Sampled current voltammograms were obtained by calculating the average current in the last 5 s of the chronoamperometric steps and plotting against the potential.

Carbon monoxide stripping analysis was performed by bubbling CO (Praxair, technical grade) vigorously onto the working electrode in the deoxygenated electrolyte for 30 min while holding it at a potential of −400 mV. The solution was then purged for 5 min with N_2 at a potential of 0.05 V followed by immediate cycling under N_2 between −100 and 1100 mV for 7 complete cycles at 10 mV s^{-1}.

For inductively coupled plasma mass spectrometry (ICP-MS) analysis, the entire electrode, minus the tab for inserting into a handle, was dissolved in *aqua regia* and evaporated to dryness on a hot plate. The residue was made up in 2% HNO_3 solution (EMD Chemicals) and submitted for analysis.

3. Results and discussion

Fig. 1 shows the potential responses of the WE (E_{WE}) and CE (E_{CE}) during the sonicated deposition of Ni–Pt on Ni gauze, Ni–Pt on Ni foam and Pt on Ni foam. Similar to our previous report [21], the changes in E_{WE} show that deposition of Ni occurs initially, and E_{CE} is sufficiently positive for Pt dissolution. Subsequently, E_{WE} rises from H_2 evolution over the deposited Pt to a value that is far above the redox potential of the Ni(0)/Ni(II) couple [21], and shortly thereafter, CE becomes passivated by surface oxides [58] ($E_{CE} \sim 1.44$ V vs. SHE, pH 5.1). In general, the rise in E_{WE} with H_2 evolution was faster and more pronounced over the Ni gauze than the Ni foam. It is likely that the differences in E_{WE} between the gauze and foam substrates arise from either the higher real surface area of the foam or a longer induction period for Pt deposition on the foam. On the other hand, for all of the depositions, the CE remained at a constant potential of 1340–1440 mV vs. SHE. For simplicity, only the E_{CE} during a Ni–Pt on Ni foam deposition was shown in Fig. 1. Based on these potential profiles we believe the mechanism of the deposition does not change significantly with the type of Ni substrate.

The average mass of eight representative Ni–Pt on Ni foam deposits was 29.8 mg with ~0.56 mg Pt (from ICP-MS). This equates to 6.0 atomic percent Pt (at.% Pt) in the Ni–Pt on Ni foam deposit, excluding the Ni inherent to the foam substrate. Six Pt on Ni foam deposits had an average mass of 0.23 mg which is consistent with ~0.21 mg Pt found from ICP-MS. These low masses are expected given the self-limiting nature of the deposition.

Fig. 2 shows SEM images of Ni gauze, Ni foam, Ni–Pt on Ni gauze, Ni–Pt on Ni foam and Pt on Ni foam. At this scale the surface of Ni–Pt on gauze (Fig. 2c) consists of thick, globular deposits while Ni–Pt on Ni foam (Fig. 2d) appears to consist of multiple thick layers. Pt on Ni foam has the thinnest deposit with the surface features of the foam substrate still visible (Fig. 2b vs. e). The Pt deposit also has a very textured surface with ridges that likely arise from the effects of H_2 evolution and sonication during the deposition. The relative roughness of the Ni–Pt deposits to the Pt only deposit is accordant with their relative masses.

Fig. 3 shows EDX mapping of Ni–Pt and Pt on Ni foam at lower magnification with ~1 μm sampling depth. At this scale, the distribution of Pt (red regions) appears uniform. ~10 at.% Pt was found in Ni–Pt on Ni foam (Fig. 3a). Given that the ICP results for Ni–Pt on Ni foam (6 at.% Pt) is less than the 10 at.% detected by EDX, then most of the Pt is at the surface of the co-deposit. This finding is consistent with the proposed self-limiting nature of the deposition. The proportion of Pt detected in the Pt on Ni foam deposit was less than 2 at.% (Fig. 3b). EDX results also showed Ni was present. This indicates that the thickness of the deposit is less than the sampling depth (1 μm) as Ni foam was detected, which is consistent with the SEM results, or parts of the Ni foam substrate remain uncovered by Pt. For both deposits a large amount, ~20–50 at.% of oxygen is present after exposure to air.

Fig. 4 shows the first and third (stabilised) cycles of baseline CVs of Ni–Pt on Ni foam and Pt on Ni foam in 0.5 M NaOH at a scan rate of 10 mV s^{-1}. We also include the stabilised CVs of the Ni foam substrate under the same conditions and the Ni blacked electrode described in Ref. [21] for comparison. The potential limits of the CVs were kept below 450 mV to prevent deeper oxidation to β-$Ni(OH)_2$ (a phase of 2 or more monolayers), which reversibly oxidises to NiOOH but does not readily reduce to zero-valent nickel [59]. (As an aside, β-$Ni(OH)_2$ has also been associated with a passivated surface that could inhibit MeOH oxidation in base [60]).

Firstly, we note the superlative increase in electro-active surface area upon comparison of bare nickel foam and the deposits. Secondly, when we compare the first cycles of the deposits to the stabilised cycles, it is evident that there is an extensive reorganization of the surface concomitant with a decrease in surface area.

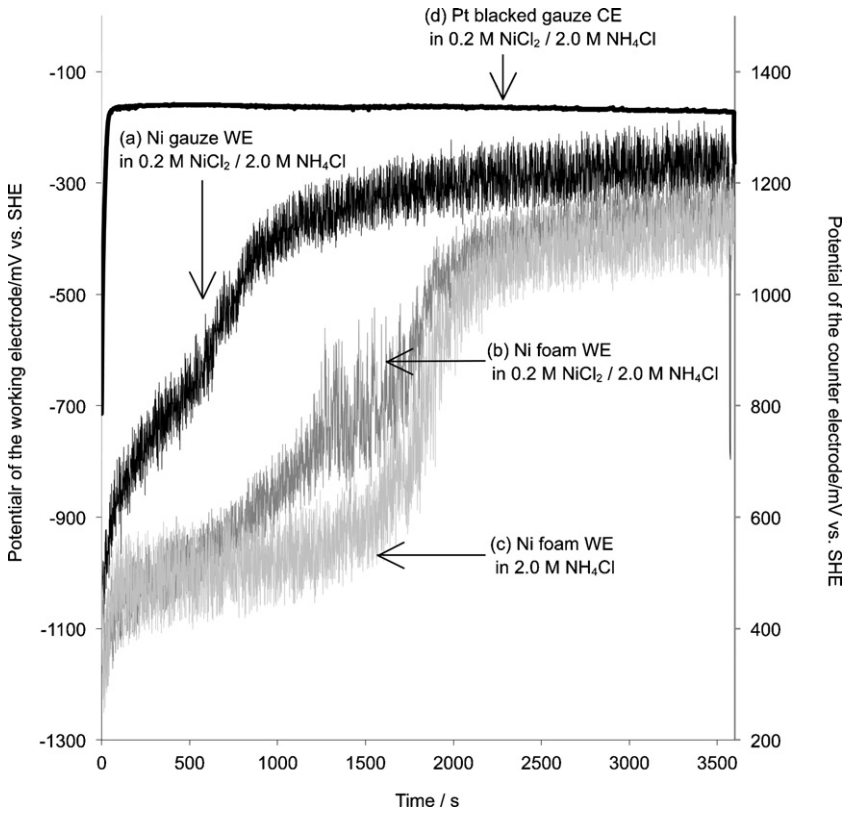

Fig. 1. Potential profiles of the electrodes during the galvanostatic deposition at −0.1 A for 1 h. (a) Ni gauze WE in 0.2 M $NiCl_2$/2.0 M NH_4Cl with a Pt CE, (b) Ni foam WE in 0.2 M $NiCl_2$/2.0 M NH_4Cl with a Pt CE, (c) Ni foam WE in 2.0 M NH_4Cl with a Pt CE, and (d) Pt blacked gauze CE in 0.2 M $NiCl_2$/2.0 M NH_4Cl with a Ni foam WE.

The charge in the first cycle is large due to the incorporation of hydrogen into the Ni during conditioning under hydrogen evolution conditions [61 and references therein].

Most interestingly, we find that the stabilised CV of Ni–Pt on Ni foam features two broad peaks between 0 and 200 mV whereas Pt on Ni foam only has one broad peak. We infer that the broad peak at about 200 mV in the Ni–Pt on Ni foam CV is due to the reversible oxidation of deposited Ni to α-$Ni(OH)_2$ (as opposed to Ni inherent to the foam substrate) despite the fact that our previous report [21] showed that this anodic peak in a Ni on Ni gauze CV appears at about 280 mV (see inset of Fig. 4a). We believe this lower overpotential for oxidising Ni is due to the presence of Pt in the deposit, that is, Pt promotes the transformation of Ni to α-$Ni(OH)_2$. In fact, if we assign the peak potential for the reduction of $Ni(OH)_2$ at ∼100 mV in the stabilised CV of Ni–Pt on Ni foam (Fig. 4a), we find that the separation of the redox peaks is much larger for Ni on Ni gauze than Ni–Pt on Ni foam indicating the apparent reaction rate must be higher in the latter. Promoter activity of small amounts of Pt in Ni–Pt catalysts is not novel; for example, Pt is thought to catalyze the reduction of nickel oxide surfaces [62,63].

The anodic peak visible at ∼50 mV in stabilised CVs of both deposits is attributed to hydrogen desorption over Pt. The peak is broad and we cannot discern between weakly and strongly adsorbed hydrogen desorption peaks. Intriguingly, this peak was also observed by Hu and Liu [64] in the first cycle of the CVs of their "Type-I" Pt deposits onto titanium substrates. Like our deposits, Type-I deposits are prepared under conditions of H_2 evolution. Hu and Liu attributed their broad anodic peak between 0 and 200 mV to the hydrogen desorption peaks on Pt as well.

The anodic charge of the Pt on Ni foam deposits was consistently smaller than that of Ni–Pt on foam. Thus the presence of deposited Ni (as opposed to Ni inherent to the foam substrate) results in a larger specific surface area deposit. This is consistent with the rougher surfaces observed in the SEM of the Ni–Pt on Ni foam co-deposits.

Fig. 5a and b shows stabilised CVs in 0.5 M NaOH and 0.5 M NaOH/1 M 2-PrOH. Both deposits are active towards 2-PrOH electro-oxidation. Fig. 5c shows the un-normalized sampled current voltammograms (SCVs) for Ni–Pt on Ni foam, Pt on Ni foam and Pt black. These were constructed from the stabilised current at the end of 15-min chronoamerometric electro-oxidations at various set potentials. The Pt black gauze SCV features an activity maximum between 100 and 250 mV. This maximum was minor for the Pt on Ni foam catalyst and absent for the Ni–Pt and Pt on foam catalysts. However, at potentials above 300 mV the deposits were very active towards the electro-oxidation, with Pt on Ni foam being the most active above 400 mV. We note that neither Ni black (synthesised by our deposition with a Ni gauze WE and a carbon CE) nor Ni foam are active towards 2-PrOH oxidation and accordingly were not included in Fig. 5c.

Specific activity of the deposits was determined by using ICP-MS data for the Ni–Pt and Pt on foam catalysts. The Pt mass-normalized currents are shown in Fig. 6. The mass-normalized data for Pt black was not included due to its mass being more than 5 orders of magnitude larger than our deposits. The results show that, above 60 mV, Pt on Ni foam was consistently higher in activity than Ni–Pt on Ni foam and therefore utilizes the mass of Pt present more efficiently. This trend is expected, in part, because some Pt would be covered by Ni during the Ni–Pt deposition.

Normalization of the current by the number of surface atoms was also attempted. The number of Pt atoms (4.47 μmol) on the Pt blacked gauze surface was calculated using the standard method of hydrogen underpotential deposition [65]. The number of surface atoms on Ni–Pt and Pt on Ni foam was estimated using CO adsorption/stripping. Fig. 7 shows the first, second and seventh stripping cycles in 0.5 M NaOH.

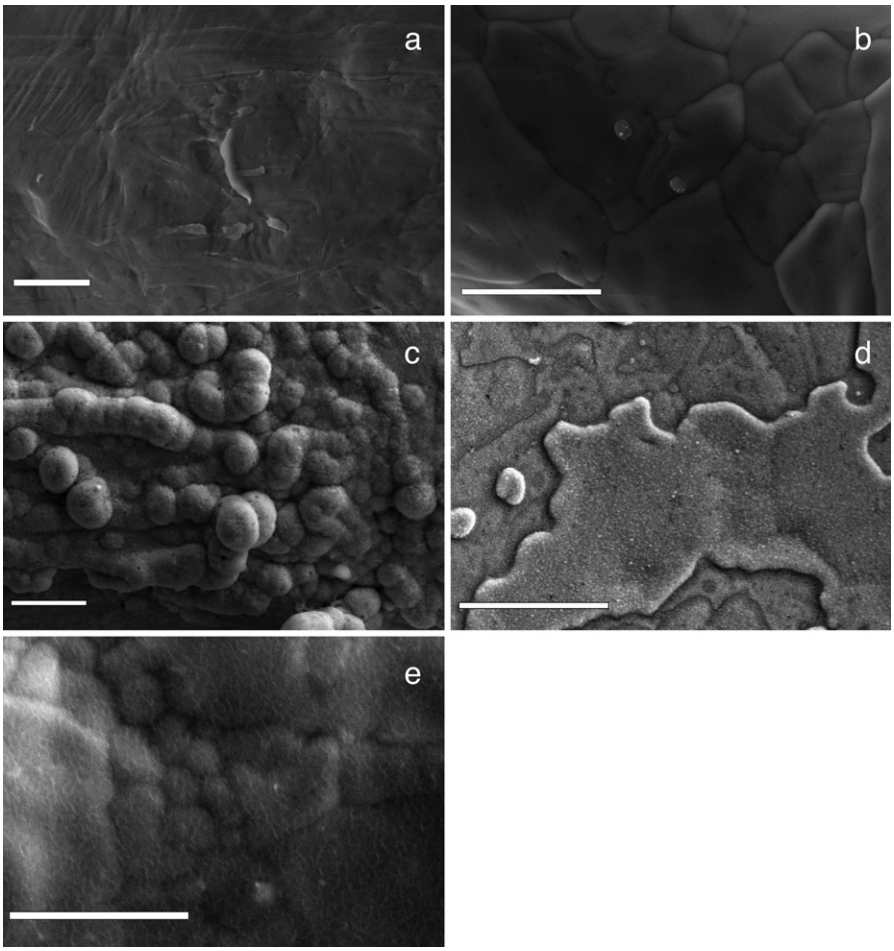

Fig. 2. Scanning electron micrographs of (a) Ni gauze, (b) Ni foam, (c) Ni–Pt on Ni gauze, (d) Ni–Pt on Ni foam, and (e) Pt on Ni foam. The scale bar is 10 μm in all images.

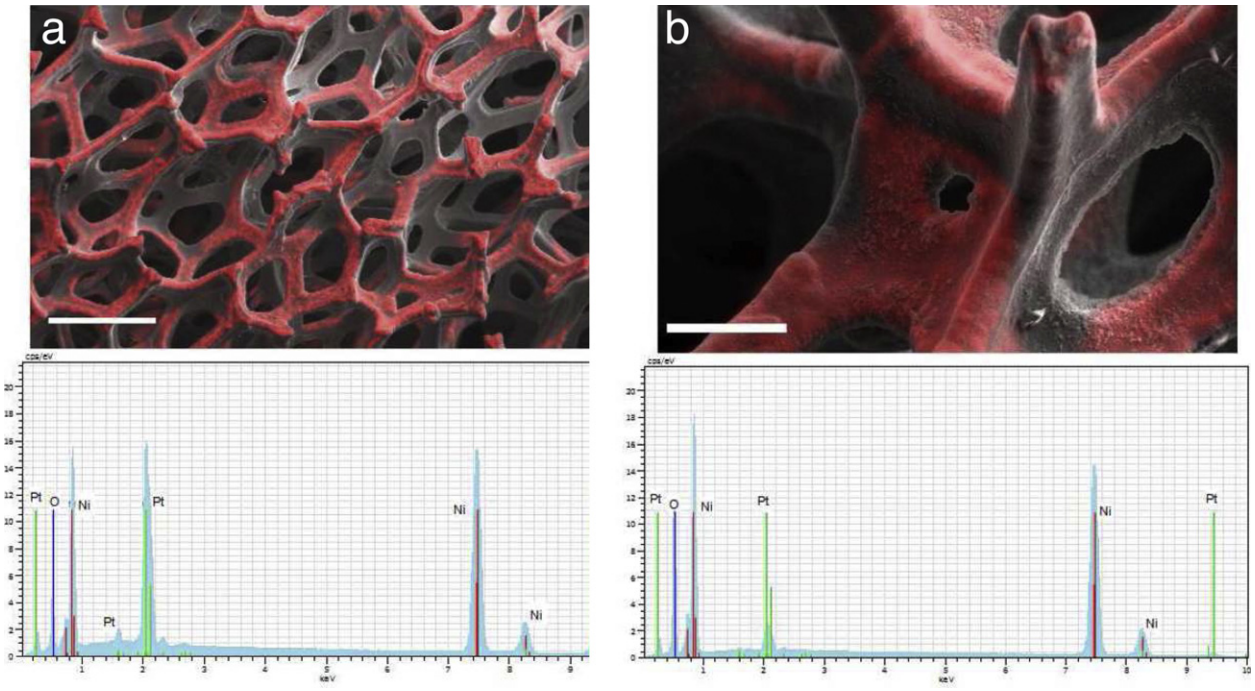

Fig. 3. EDX mapping of Pt (red) on the surface of the deposits: (a) Ni–Pt on Ni foam, scale bar 300 μm and (b) Pt on Ni foam, scale bar 70 μm. (For interpretation of the references to colour in this figure legend, the reader is referred to the web version of the article.)

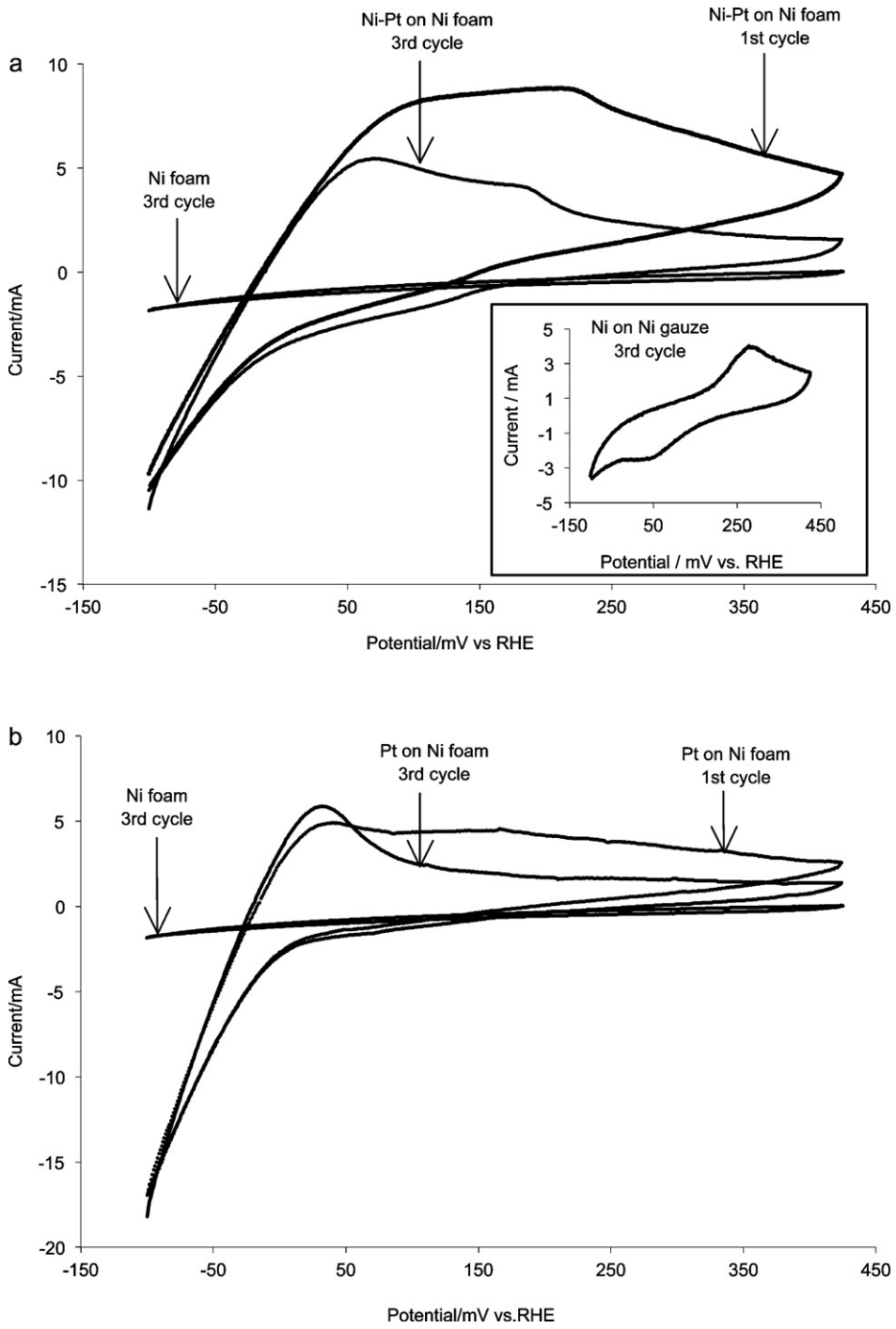

Fig. 4. Cyclic voltammograms in 0.5 M NaOH at 22 °C with a scan rate of 10 mV s^{-1}. (a) Ni foam, 3rd (stabilised) cycle (dotted line), Ni–Pt on Ni foam, 1st cycle (dotted line) and Ni–Pt on Ni foam, 3rd (stabilised) cycle (solid line); inset: Ni on Ni gauze as prepared in Ref. [21]. (b) Ni foam, 3rd (stabilised) cycle (dotted line), Pt on Ni foam, 1st cycle (dotted line) and Pt on Ni foam, 3rd (stabilised) cycle (solid line).

Given the evolution of the voltammograms we propose the following: the anodic charge of the 1st cycle is the combined charge of the 2 electron oxidation of adsorbed CO to CO_2, the irreversible 2 electron oxidation of Ni to β-$Ni(OH)_2$, and double layer capacitance; the anodic charge of the 2nd cycle results from double layer capacitance and further oxidation of Ni to β-$Ni(OH)_2$ until the Ni surface is mostly, if not entirely passivated; finally, the 7th cycle is purely capacitative current. Therefore, the combined charge due to CO stripping and the Ni surface oxidation, Q_{TOT}, represents a 4 electron process and is given by Eq. (3):

$$\begin{aligned} Q_{TOT} &= [CO_{ads}\ \text{oxidation charge} + \text{Ni surface oxidation charge}] \\ &= [(\text{anodic charge of cycle 1}) + (\text{anodic charge of cycle 2})] \\ &\quad - 2(\text{anodic charge of cycle 7}) \end{aligned} \tag{3}$$

The number of surface atoms would therefore be given by $Q_{TOT}/4F$ where F is Faraday's constant, 96,485 C mol^{-1}. Assuming that CO is adsorbed on both Ni and Pt surface atoms, and that Ni oxidation is likely for many surface layers, we acknowl-

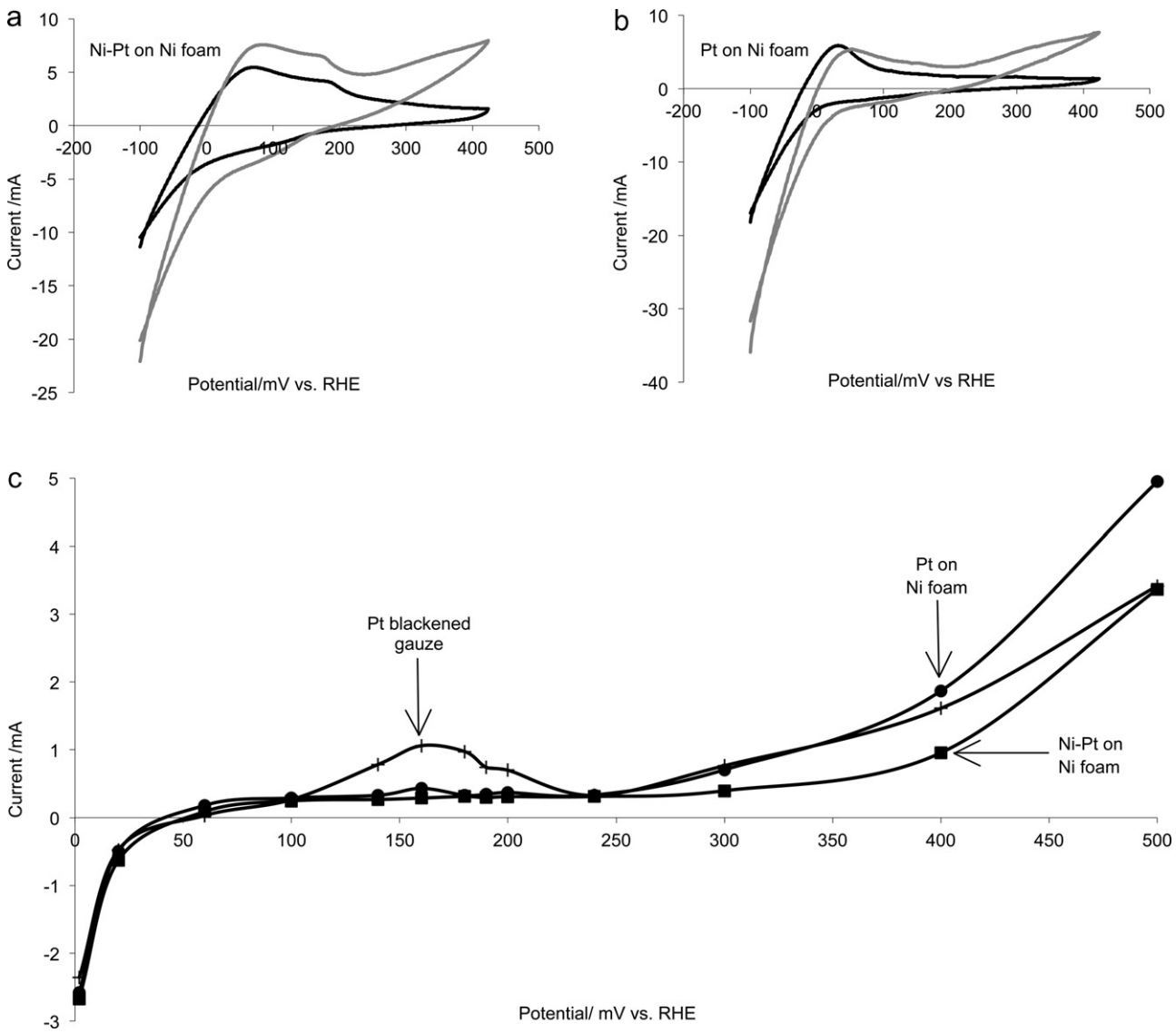

Fig. 5. (a) Cyclic voltammograms of Ni–Pt on Ni foam in 0.5 M NaOH at 22 °C (black line) and in 0.5 M NaOH/1.0 M 2-PrOH at 60 °C (grey line) at 10 mV s^{-1}; (b) cyclic voltammograms of Pt on Ni foam in 0.5 M NaOH at 22 °C (black line) and in 0.5 M NaOH/1.0 M 2-PrOH at 60 °C (grey line) at 10 mV s^{-1}; (c) un-normalized sampled current voltammograms in 0.5 M NaOH/1.0 M 2-PrOH at 60 °C for Ni–Pt on Ni foam (solid squares), Pt on Ni foam (solid circles) and Pt blackened gauze (+).

edge that our calculation would be an over-estimate as the number of surface atoms of Ni is likely accounted for multiple times.

We did not use a particular sample for both CO stripping and 2-PrOH electro-oxidation because the catalyst surface will be permanently changed at the potential limits used in CO stripping. Therefore, we assumed that two of the same type of electrode with similar anodic charge, Q_{CV}, in their stabilised base CVs (as seen in Fig. 4) should have similar activity towards 2-PrOH. As a result, we combined raw activity data of a particular electrode (denoted A) with CO stripping data of another electrode (denoted B) using Eq. (4):

$$\text{No. of moles of surface atoms} = \frac{f \cdot Q_{TOT}}{4F} \quad (4)$$

where the standardization factor, f, is defined as the ratio of Q_{CV} of electrode B to electrode A. Table 1 summarizes the data used to produce the surface-atom normalized SCVs for Pt black, Ni–Pt, and Pt on Ni foam shown in Fig. 8.

The normalized activities of the Ni–Pt, and Pt on Ni foam towards 2-PrOH were not significantly greater than Pt black between 50 and 250 mV. This result is similar to or previous results for the Ni–Pt on gauze catalyst. However, our catalysts were markedly more active than Pt at potentials higher than 250 mV. The improvement ranged from 9 to 37 times at 500 mV. Pt on Ni foam had the highest surface atom normalized activity above 50 mV, followed by Ni–Pt on Ni foam; Pt black had the worst performance in this potential range. These results confirm that Ni promotes 2-PrOH electro-oxidation, particularly at high potentials where the oxidation of the intermediate acetone also occurs.

The electronic influence of the Ni on Pt was investigated by XPS. Fig. 9 shows the Pt 4*f* XPS spectra of Ni–Pt and Pt on Ni foam. The

Table 1
Summary of surface atom calculations for normalization of activity data by number of surface atoms.

Electrode	Q_{CV} (C)	Q_{TOT} (C)	f[a]	No. of surface atoms (μmol)
Ni–Pt on Ni foam B	0.087	0.286	0.65	0.480
Pt on Ni foam B	0.074	0.090	0.74	0.173

[a] The anodic charges of the base cyclic voltammograms of Ni–Pt on Ni foam A and Pt on Ni foam A were 0.134 and 0.100 C respectively.

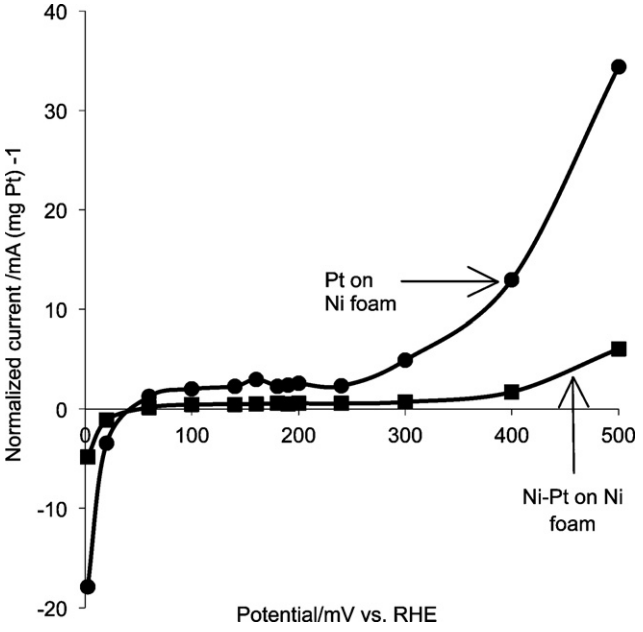

Fig. 6. Pt-mass normalized sampled current voltammograms in 0.5 M NaOH/1.0 M 2-PrOH at 60 °C for Ni–Pt on Ni foam (solid squares) and Pt on Ni foam (solid circles).

Table 2
Calculated average and experimental binding energies and standard deviations.

Chemical state and spectral line	Binding energy (eV)		
	Reference	Ni–Pt on Ni foam	Pt on Ni foam
Pt[a] $4f_{7/2}$	71.1 (0.1)[b]	70.8	71.3
$Pt(OH)_2$ $4f_{7/2}$	72.7 (0.1)	72.7	73.2
Pt(II) $4f_{7/2}$	73.8	–	–
Pt(IV) $4f_{7/2}$	74.6	–	–
NiO[c] $3p_{3/2}$	68.0 (–)	67.2	67.6
$Ni(OH)_2$ $3p_{3/2}$	69.0 (–)	69.2	69.3

[a] Specimens were either Pt crystals or sputtered platinum samples.
[b] Numbers in brackets denote the standard deviation of the data set for values in the reference column. In all other columns experimental error was ±0.1 eV. Dashes in brackets signify that no standard deviation has been recorded as only one value for the spectral line has been reported in the database.
[c] Specimens were pelletized crystals or films.

Table 3
Chemical states and area ratios of Ni–Pt and Pt on Ni foam catalysts by XPS.

Chemical state	XPS area ratio (%)	
	Ni–Pt on Ni foam	Pt on Ni foam
Pt	32.08	29.96
NiO	25.65	33.61
$Ni(OH)_2$	31.12	24.04
$Pt(OH)_2$	11.13	12.40

general shape of both spectra have the following features: (i) a Pt 4*f* doublet with peaks at ~71 and 74 eV, (ii) asymmetric tails on these doublets at higher binding energies, and (iii) a large Ni 3*p* shoulder at ~69 eV. The asymmetric tails in the spectra indicate the presence of metal atoms with nearly zero charge [66]. To fit the other two features we used four pairs of peaks representing metallic Pt, $Pt(OH)_2$, NiO and $Ni(OH)_2$ based on reported data [57]. The choice of these peaks is based on the position of the experimental peaks (Table 2) and upon the presence of a large amount of oxygen on the surface of our catalysts as seen in a survey spectrum.

The XPS area ratios indicate that Ni–Pt on Ni foam has >30% Pt. Given that XPS probes depths of 3–9 nm, and comparing these results to those from EDX (10 at.% Pt), and ICP-MS (6 at.% Pt), then most of the deposited Pt is on or near the surface. With this in mind we believe the best model for the Ni–Pt on Ni foam catalyst is gradually decreasing proportions of platinum in a bimetallic Pt and Ni shell with a nickel foam core.

With respect to Ni–Pt on Ni foam, the Pt metal $4f_{7/2}$ peak appeared at 70.8 ± 0.1 eV. The peaks shifted to a slightly lower binding energy (BE) compared to the expected experimental BE for Pt bulk, 71.1 eV, given in Table 2. Given the absence of Pt 4*f* peak values for Pt(II) (excluding $Pt(OH)_2$) and Pt(IV) species [48,57], and the relative areas of the Pt metal peaks to the $Pt(OH)_2$ peaks, shown in Table 3, the majority of the Pt exists in an oxidation state closer to 0 than to +2. We note that the magnitude of the shift is within the range of 3 standard deviations of the bulk value making the effect observed small.

In the case of the Pt on Ni foam catalysts, the Pt metal $4f_{7/2}$ peak appeared at 71.3 ± 0.1 eV, a slightly positive shift with respect

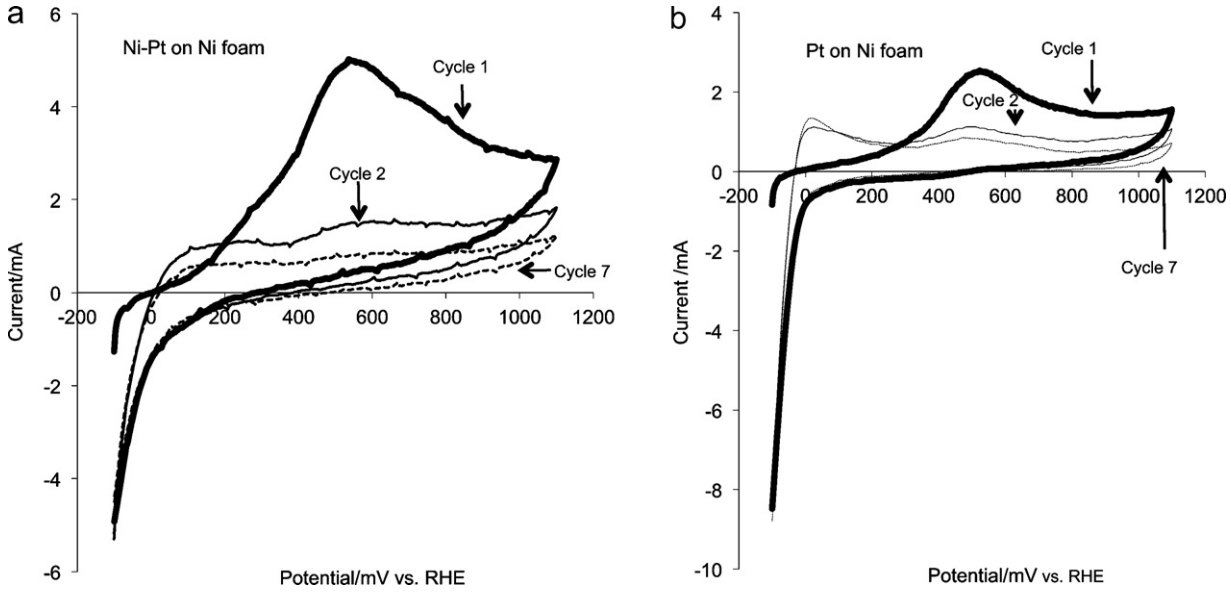

Fig. 7. Cyclic voltammogram cycles 1, 2 and 7 of carbon monoxide stripping in 0.5 M NaOH at 10 mV s^{-1}. Prior to stripping, the carbon monoxide was adsorbed at −400 mV vs. RHE for 30 min followed by purging with nitrogen for 5 min at 500 mV vs. RHE. (a) Ni–Pt on Ni foam and (b) Pt on Ni foam.

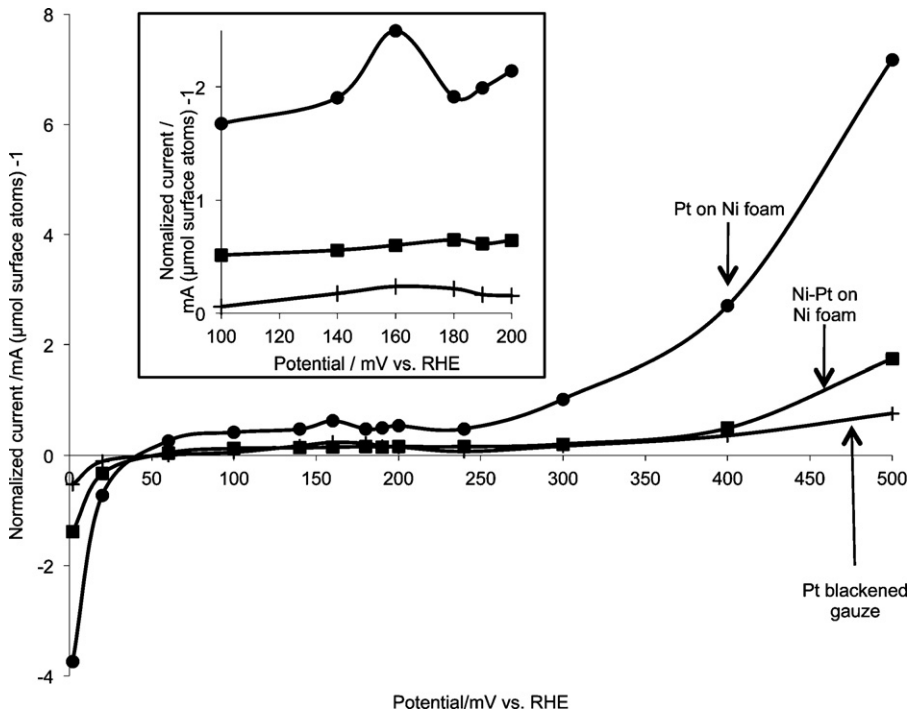

Fig. 8. Surface area normalized sampled current voltammograms in 0.5 M NaOH/1.0 M 2-PrOH at 60 °C for Ni–Pt on Ni foam (solid squares), Pt on Ni foam (solid circles) and Pt blackened gauze (+). Inset is the same within the range of 100–200 mV vs. RHE.

to bulk Pt and opposite in direction of the Ni–Pt on foam catalyst. However, we point out that the shift is within 2 standard deviations of the Pt bulk value, so it is either very small or inconsequential.

The interpretations of previously reported XPS analyses of Ni–Pt systems vary. For example Toda et al. observed positive BE shifts with respect to pure Pt in their Ni–Pt alloys with Pt-rich surfaces [41]. They suggested that the shift originated from either an increase in the *d* vacancies in the *d* orbitals of the surface Pt as a result of alloying with Ni which has more 5*d* vacancies than Pt, or a lowering of the Fermi level on Pt. In contrast, both Papadimitirou et al. [32] and Park et al. [27,40] reported negative shifts in BE in their Ni–Pt coatings and thin films/nanoparticles respectively. Papadimitirou and his peers attributed the observed shift to the lowering of the *d* band center and not to the occupation of states or proportion of *d* vacancies at the Fermi level on Pt in the presence of Ni. They suggested further that if the alloying metal was less electronegative than Pt, it would donate electron density to Pt and cause a lowering in the energy of the *d* band center. Park and co-workers attributed their negative shifts to an electron transfer from Ni to Pt and proposed that the higher the degree of alloying in their catalysts the larger the absolute XPS shift. Both groups associated the lowering of the *d* band center with lowered affinity of Pt for

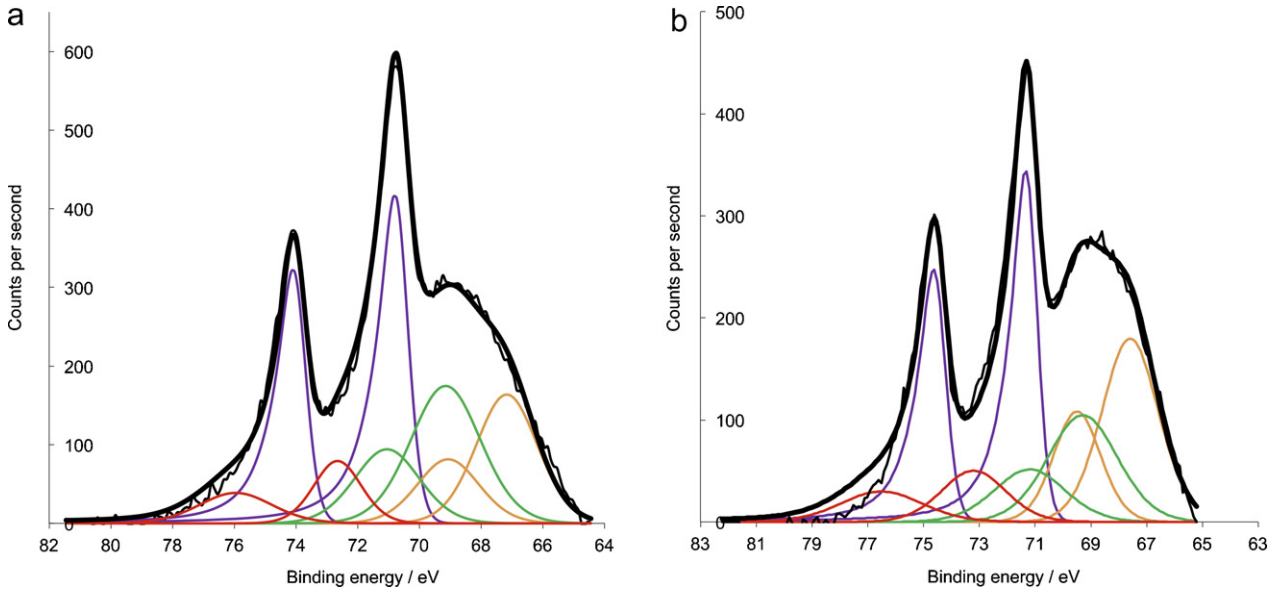

Fig. 9. Pt 4*f* X-ray photoelectron spectra for (a) Ni–Pt on Ni foam and (b) Pt on Ni foam deposits. Fitting lines are Pt (purple), $Pt(OH)_2$ (red), $Ni(OH)_2$ (green) and NiO (orange). (For interpretation of the references to colour in this figure legend, the reader is referred to the web version of the article.)

adsorbates such as CO. The commonality amongst these reports is that the authors did not account for observed activity trends solely with electronic effects.

With respect to Ni–Pt on Ni foam catalyst, we suggest a few possibilities for the origin of the observed shifts to lower BE. Based on the Allred–Rochow electronegativity (EN) scale [67], Pt is less electronegative than Ni [68]. We believe this scale is more appropriate for the XPS experiment as it describes the attraction between the electron and the nucleus of the bonded atom. As Pt is less electronegative, it is possible that Ni is donating 5*d* vacancies to Pt as suggested by Toda et al. [41] or Pt is donating electron density to Ni. The Fermi level of the Pt would lie closer to the center of the valence band, analogous to the effect of p-doping in a semiconductor [69]. It follows that the observed BE would be smaller than that of bulk Pt.

This shift to lower BE is correlated to weaker bond strength between Pt and different adsorbates as suggested independently by Papadimitirou et al. [32] and Park et al. [27,40] and in general by Nørskov and co-workers [43]. This would imply that the adsorption of species onto Ni–Pt on foam is weaker than onto Pt on Ni foam or Pt black. In fact, we did find that CO may be more weakly adsorbed on Ni–Pt on Ni foam than Pt on Ni foam as it had a lower CO stripping onset potential than the latter (Fig. 7). Furthermore, the onset potential of CO stripping on Pt (1 0 0) and Pt (1 1 1) is at least ~200 and 450 mV higher than on our Ni–Pt on Ni foam and Pt on Ni foam deposits [70,71].

On a similar notion, this trend in BE could account for the low potential current maximum attributed to acetone inhibition seen in the SCVs (Figs. 5c and 6 and especially the inset of Fig. 8); this feature was almost absent for Ni–Pt on Ni foam. At these potentials the activation of 2-PrOH as well as acetone inhibition would be reliant on the autonomous adsorption of the two molecules on the catalyst surface. Ni–Pt should therefore have the weakest adsorption properties according to the XPS and this is consistent with the lowest current maximum (that is the absolute difference between the current at 100 and 160 mV). This concept is, to some extent, related to that seen in Ref. [32] wherein both MeOH fuel and CO poison adsorption was affected by the lowering of the energy of the *d* band center. Depending on the time-scale of the experiment independent adsorption of the molecules was affected to different degrees, such that at short times, when MeOH activation was the major pathway, Pt was more active than Ni–Pt and at long times, when CO poisoning was prominent, Ni–Pt was more active than Pt.

If the positive XPS shift observed in our Pt on Ni foam is not significant, then the Pt in this deposit is electronically similar to bulk Pt. Consequentially, electronic effects would not sufficiently explain the activity enhancement of this catalyst especially at potentials above 250 mV where Pt black is the worst performer and Pt on Ni foam is the best performer.

We generated Tafel plots from the mass-normalized data in Fig. 6 and found that the Tafel slopes above 200 mV were 263, 227 and 250 mV dec^{-1} on Pt black, Pt on Ni foam and Ni–Pt on Ni foam respectively. The values are all comparable, indicating the mechanism of 2-PrOH/acetone oxidation over the three electrodes are likely similar. We also remind the reader that neither Ni foam nor Ni black appreciably catalyze this reaction. In light of these findings, we believe that the presence of Ni in both of our catalysts improves the activity of Pt at high potentials mainly via the bi-functional mechanism and less by an electronic effect. The mechanism of 2-PrOH oxidation discussed in Section 1 is such that addition of Ni to Pt enhances the current observed only at potentials >250 mV [21]. It is apparent, therefore, that Ni promotes the electro-oxidation only after it is converted to $Ni(OH)_2$ and OH is provided to commence the bi-functional mechanism. This is similar to suggestions by Park et al. that oxides on Ni can act as oxygen donors in a surface redox process that removes CO poisons during methanol oxidation at long times [27,40]. We also wish to reiterate that the onset potentials in our CO stripping experiments were lower than what was observed for Pt [70,71] which provides further evidence that a bi-functional mechanism is indeed probable on our electrodes.

It is interesting that Pt on Ni foam is more active than Ni–Pt on Ni foam at potentials above 250 mV despite the latter having a higher Ni content and likely a greater bi-functional effect. Perhaps a geometric effect similar to the one described by Yang et al. in Ref. [28] is existent for Pt on Ni foam. Given it is not co-deposited, the probability of having enough Pt sites in the correct orientation for 2-PrOH adsorption is much higher than in Ni–Pt on Ni foam. It is therefore highly likely that this additional geometric effect makes Pt on Ni foam so much more active than Ni–Pt on Ni foam, and the combination with the bi-functional effect makes it superior to Pt black. We also should not discount the possibility that the deposition itself creates a highly active form of Pt.

4. Conclusions

We present a microscopic, spectroscopic and electrochemical study of Ni–Pt and Pt supported on Ni foam for 2-PrOH electrooxidation in base. We have shown that our unique galvanostatic self-limiting co-deposition of nickel and platinum occurs under conditions of sonication and produces deposits with ultra-low platinum loadings on nickel foam. We have also demonstrated that our technique can be used to deposit small amounts of Pt onto nickel foam substrates. Most of the Pt in the Ni–Pt on Ni foam was found to reside near the deposit surface.

The co-deposits, Ni–Pt on Ni foam and Ni–Pt and Ni gauze, had rougher surfaces than Pt on Ni foam. This reflected the relative masses of the deposits as well as the relative charges in their CVs in base. CVs also revealed that Ni–Pt on Ni foam had both nickel and platinum characteristics, while only Pt peaks were identified for Pt on Ni foam. Both deposits were active towards 2-PrOH electrooxidation in base and showed higher activity than Pt black when normalized to the estimated number of surface atoms; the order of activity at 500 mV was Pt black < Ni–Pt on Ni foam $\ll$ Pt on Ni foam.

Electronic effects were more apparent on the Pt in Ni–Pt on Ni foam while any XPS shift for Pt on Ni foam was negligible. The observed activity at potentials between 50 and 250 mV were attributed to electronic effects in the Ni–Pt on Ni foam catalysts. We believe that the enhanced activity at potentials >250 mV for Ni–Pt on Ni foam was a combination of electronic and bi-functional effects and for Pt on Ni foam a combination of geometric and bi-functional effects. Further investigations are underway in this laboratory to gain some insight on these phenomena. Future work also includes using these deposits as oxygen reduction catalysts and to promote other alcohol oxidations.

Acknowledgements

The National Science and Engineering Research Council of Canada, Canada School of Energy and Environment, and the University of Alberta supported this research. We thank GeoChem Technician Guangcheng Chen and SEM Lab Technician De-Ann Rollings of the Earth and Atmospheric Sciences Department at the University of Alberta for ICP-MS and SEM/EDX data collection. We also thank Shihong Xu and Dr. Anquang He of the Alberta Centre for Surface Engineering and Science for performing XPS analysis and Peter Blanchard for assistance with interpretation of XPS results.

References

[1] M.E.P. Markiewicz, S.H. Bergens, J. Power Sources 195 (2010) 7196–7201.
[2] C. Lamy, A. Lima, V. Le Rhun, F. Delime, C. Coutanceau, J.-M. Léger, J. Power Sources 105 (2002) 283–296.

[3] J.R. Varcoe, R.C.T. Slade, Fuel Cells 5 (2005) 187–200.
[4] P. Millet, A. Michas, R.J. Durand, Appl. Electrochem. 26 (1996) 933–937.
[5] K.-C. Kim, S.M. Cho, H.-G. Choi, Sens. Actuators B 67 (2000) 194–198.
[6] V. Bambagioni, C. Bianchini, A. Marchionni, J. Filippi, F. Vizza, J. Teddy, P. Serp, M. Zhiani, J. Power Sources 190 (2009) 241–251.
[7] C. Bianchini, V. Bambagioni, J. Filippi, A. Marchionni, F. Vizza, P. Bert, A. Tampucci, Electrochem. Commun. 11 (2009) 1077–1080.
[8] A. Serov, C. Kwak, Appl. Catal. B 97 (1–2) (2010) 1–12.
[9] M. Simões, S. Baranton, C. Coutanceau, Appl. Catal. B 93 (2010) 354–362.
[10] J. Liu, J. Ye, C. Xu, S.P. Jiang, Y. Tong, J. Power Sources 177 (2008) 67–70.
[11] T. Kobayashi, J. Otomo, C.-J. Wen, H. Takahashi, J. Power Sources 124 (2003) 34–39.
[12] D. Cao, S.H. Bergens, J. Power Sources 124 (2003) 12–17.
[13] Y. Su, C. Xu, J. Liu, Z. Liu, J. Power Sources 194 (2009) 295–297.
[14] C. Xu, Z. Tian, Z. Chen, S.P. Jiang, Electrochem. Commun. 10 (2008) 246–249.
[15] J. Ye, J. Liu, C. Xu, S.P. Jiang, Y. Yong, Electrochem. Commun. 9 (2007) 2760–2763.
[16] M.E.P. Markiewicz, S.H. Bergens, J. Power Sources 185 (2008) 222–225.
[17] M.E.P. Markiewicz, D.M. Hebert, S.H. Bergens, J. Power Sources 161 (2006) 761–767.
[18] A. Santasalo, F.J. Vidal-Iglesias, J. Solla-Gullón, A. Berná, T. Kallio, J.M. Feliu, Electrochim. Acta 54 (2009) 6576–6583.
[19] I.A. Rodrigues, F.C. Nart, J. Electroanal. Chem. 590 (2006) 145–151.
[20] E. Bingham, B. Cohrssen, C.H. Powell, Patty's Toxicology, 5th ed., John Wiley & Sons, New Jersey, 2001, Online version (last accessed 18.11.10), http://knovel.com/web/portal/browse/display?_EXT_KNOVEL_DISPLAY_bookid=706&VerticalID=0.
[21] L.N. Menard, S.H. Bergens, J. Power Sources 194 (2009) 298–302.
[22] M. Watanabe, S. Mootoo, J. Electroanal. Chem. 60 (1975) 267–273.
[23] B. Gurau, R. Viswanathan, R. Liu, T.J. Lafrenz, K.L. Ley, E.S. Smotkin, E. Reddington, A. Sapienza, B.C. Chan, T.E. Mallouk, S. Sarangapani, J. Phys. Chem. B 102 (1998) 9997–10003.
[24] T. Frelink, W. Visscher, A.P. Cox, J.A.R. van Veen, Electrochim. Acta 39 (1994) 1871–1875.
[25] T. Frelink, W. Visscher, J.A.R. van Veen, Electrochim. Acta 40 (1995) 1537–1543.
[26] E. Pastor, S. González, A.J. Arvia, J. Electroanal. Chem. 395 (1995) 233–242.
[27] K.W. Park, J.-H. Choi, Y.-E. Sung, J. Phys. Chem. B 107 (2003) 5851–5856.
[28] H. Yang, C. Coutanceau, J.-M. Léger, N. Alonso-Vante, C. Lamy, J. Electroanal. Chem. 576 (2005) 305–313.
[29] J. Zhang, J. Fang, J. Am. Chem. Soc. 131 (2009) 18543–18547.
[30] X.-Z. Fu, Y. Liang, S.-P. Chen, J.-D. Lin, D.-W. Lia, Catal. Commun. 10 (2009) 1893–1897.
[31] N.H.H. Abu Bakar, M.M. Bettahar, M. Abu Bakar, S. Monteverdi, J. Ismail, M. Alnot, J. Catal. 265 (2009) 63–71.
[32] S. Papadimitirou, S. Armyanov, E. Valova, A. Hubin, O. Steenhaut, E. Pavlidou, G. Kokkinidis, S. Sotiropoulos, J. Phys. Chem. C 114 (2010) 5217–5223.
[33] E. Antolini, J.R.C. Salgado, A.M. dos Santos, E.R. Gonzalez, Electrochem. Solid-State Lett. 8 (2005) A226–A230.
[34] R.R. Hoover, Y.V. Tomalchev, J. Electrochem. Soc. 156 (2009) A37–A43.
[35] Y. Chen, F. Yang, Y. Dai, W. Wang, S. Chen, J. Phys. Chem. C 112 (2008) 1645–1649.
[36] A. Tegou, S. Papadimitriou, G. Kookinidis, S. Sotiropoulous, J. Solid State Electrochem. 14 (2010) 175–184.
[37] V. Stamenković, T.J. Schmidt, P.N. Ross, N.M. Marković, J. Phys. Chem. B 106 (2002) 11970–11979.
[38] V.R. Stamenkovic, B.S. Mun, K.J.J. Mayrhofer, P.N. Ross, N.M. Marković, J. Am. Chem. Soc. 128 (2006) 8813–8819.
[39] P.C.H. Mitchell, P. Woloman, D. Thompson, S.J. Cooper, J. Mol. Catal. A: Chem. 119 (1997) 223–233.
[40] K.-W. Park, J.-H. Choi, B.-K. Kwon, W.-A. Lee, Y.-E. Sung, H.-Y. Ha, S.-A. Hong, H. Kim, A.J. Wieckowski, Phys. Chem. B 106 (2002) 1869–1877.
[41] T. Toda, H. Igarashi, H. Ushida, M. Watanabe, J. Electrochem. Soc. 146 (1999) 3750–3756.
[42] H. Yang, C. Coutanceau, J.-M. Léger, N. Alonso-Vante, C.J. Lamy, Electroanal. Chem. 576 (2005) 305–313.
[43] J.R. Kitchin, J.K. Nørskov, M.A. Barteau, J.G. Chen, J. Chem. Phys. 120 (2004) 10240–10246.
[44] U.A. Paulus, A. Wokaun, G.G. Scherer, T.J. Schmidt, V. Stamenkovic, V. Radmilovic, N.M. Marković, P.N. Ross, J. Phys. Chem. B 106 (2002) 4181–4191.
[45] U.A. Paulus, A. Wokaun, G.G. Scherer, T.J. Schmidt, V. Stamenkovic, N.M. Marković, P.N. Ross, Electrochim. Acta 47 (2002) 3787–3798.
[46] V. Stamenković, T.J. Schmidt, P.N. Ross, N. Marković, J. Phys. Chem. B 106 (2002) 11970–11979.
[47] V.R. Stamenkovic, B. Fowler, B.S. Mun, G. Wang, P.N. Ross, C.A. Lucas, N.M. Marković, Science 315 (2007) 493–497.
[48] R. Mu, Q. Fu, H. Xu, H. Zhang, Y. Huang, Z. Jiang, S. Zhang, D. Tan, X. Bao, J. Am. Chem. Soc. 133 (2011) 1978–1986.
[49] J. Mathiyarasu, A.M. Remona, A. Mani, K.L.N. Phani, V. Yegnaraman, J. Solid State Electrochem. 8 (2004) 968–975.
[50] T. Frelink, W. Visscher, J.A.R. van Veen, J. Electroanal. Chem. 382 (1995) 65–72.
[51] P.A. Christensen, A. Hamnett, J. Munk, G.L. Troughton, J. Electroanal. Chem. 370 (1994) 251–258.
[52] J.M. Skowroński, A. Wazny, J. Solid State Electrochem. 9 (2005) 890–899.
[53] D. Cao, D. Chen, J. Lan, G. Wang, J. Power Sources 190 (2009) 346–350.
[54] W. Yang, S. Yang, W. Sun, G. Sun, Q. Xin, Electrochim. Acta 52 (2006) 9–14.
[55] J. Kilma, Ultrasonics 51 (2011) 202–209.
[56] U.S. Patent No. 4,750,977 (issued June 14, 1988).
[57] C.D. Wagner, A.V. Naumkin, A. Kraut-Vass, J.W. Allison, C.J. Powell, J.R. Rumble Jr., NIST X-ray Photoelectron Spectroscopy Database, Version 3.5 (Web Version), National Institute of Standards and Technology, Gaithersburg, MD, 2003 (srdata.nist.gov/xps).
[58] Y. Xu, M. Shao, M. Mavrikakis, R.R. Adzic, in: A. Wieckowski, M.T.M. Koper (Eds.), Fuel Cell Catalysis—A Surface Science Approach, John Wiley and Sons, Inc., New Jersey, 2009, pp. 271–315.
[59] B. Beden, D. Floner, J.M. Léger, C. Lamy, Surf. Sci. 162 (1985) 822–829.
[60] M.A. Abdel Rahim, H.B. Hassan, R.M. Abdel Hameed, Fuel Cells 07 (2007) 298–305.
[61] S.A.S. Machado, J. Tiengo, P. De Lima Neto, L.A. Avaca, Electrochim. Acta 39 (1994) 1757.
[62] E.J. Nowak, R.M. Koros, J. Catal. 7 (1967) 50–56.
[63] N.V. Parizotto, D. Zanhet, K.O. Rocha, C.M.P. Marques, J.M.C. Bueno, Appl. Catal. A 366 (2009) 122–129.
[64] C. Hu, K. Liu, Electrochim. Acta 44 (1999) 2727–2738.
[65] T.J. Schmidt, H.A. Gasteiger, G.D. Stäb, P.M. Urban, D.M. Kolb, R.J. Behm, J. Electrochem. Soc. 145 (1998) 2354–2358.
[66] A.P. Grosvenor, S.D. Wik, R.G. Cavell, A. Mar, Inorg. Chem. 44 (2005) 8988–8998.
[67] A.L. Allred, E.G. Rochow, J. Inorg. Nucl. Chem. 5 (1958) 264–268.
[68] J.E. Huheey, Inorganic Chemistry: Principles of Structure and Reactivity, 3rd ed., Harper and Row, New Yorok, 1983, pp.146–148.
[69] D. Dobler, S. Oswald, K. Wetzig, Anal. Bioanal. Chem. 374 (2002) 646–649.
[70] G. García, M.T.M. Koper, Phys. Chem. Chem. Phys. 10 (2008) 3802–3811.
[71] D.F. van der Vliet, M.T.M. Koper, Surf. Sci. 604 (2010) 1912–1918.